ARMY RESEARCH LABORATORY

Developing NanoFoil-Heated Thin-Film Thermal Battery

by Michael S. Ding, Frank C. Krieger, and Jeffrey A. Swank

ARL-TR-6664 **September 2013**

NOTICES

Disclaimers

The findings in this report are not to be construed as an official Department of the Army position unless so designated by other authorized documents.

Citation of manufacturer's or trade names does not constitute an official endorsement or approval of the use thereof.

Destroy this report when it is no longer needed. Do not return it to the originator.

Army Research Laboratory
Adelphi, MD 20783-1197

ARL-TR-6664 **September 2013**

Developing NanoFoil-Heated Thin-Film Thermal Battery

Michael S. Ding, Frank C. Krieger, and Jeffrey A. Swank
Sensors and Electron Devices Directorate, ARL

REPORT DOCUMENTATION PAGE

Form Approved
OMB No. 0704-0188

1. REPORT DATE *(DD-MM-YYYY)*	2. REPORT TYPE	3. DATES COVERED (From - To)
September 2013		

4. TITLE AND SUBTITLE
Developing NanoFoil-Heated Thin-Film Thermal Battery

5a. CONTRACT NUMBER

5b. GRANT NUMBER

5c. PROGRAM ELEMENT NUMBER

6. AUTHOR(S)
Michael S. Ding, Frank C. Krieger, and Jeffrey A. Swank

5d. PROJECT NUMBER

5e. TASK NUMBER

5f. WORK UNIT NUMBER

7. PERFORMING ORGANIZATION NAME(S) AND ADDRESS(ES)
U.S. Army Research Laboratory
ATTN: RDRL-SED-C
2800 Powder Mill Road
Adelphi, MD 20783-1197

8. PERFORMING ORGANIZATION REPORT NUMBER
ARL-TR-6664

9. SPONSORING/MONITORING AGENCY NAME(S) AND ADDRESS(ES)

10. SPONSOR/MONITOR'S ACRONYM(S)

11. SPONSOR/MONITOR'S REPORT NUMBER(S)

12. DISTRIBUTION/AVAILABILITY STATEMENT
Approved for public release; distribution unlimited.

13. SUPPLEMENTARY NOTES

14. ABSTRACT
This report describes and discusses a series of experiments in which aluminum-nickel NanoFoil materials were used as the heat source for other thermal battery components, such as cathode, anode, and electrolyte, in the form of coated thin films, to develop a NanoFoil-heated thin-film thermal battery technology. This work culminated in the design, construction, and characterization of a complete, fully functional 12-cell NanoFoil-heated thin-film thermal battery prototype, which demonstrated a much faster rise in working voltage, a much lower internal gas pressure, a much shorter stack height, and a much greater flexibility in form factor, than the traditional pressed-pellet thermal batteries. In the process of screening and optimizing for the NanoFoil-heated thin-film thermal battery prototype, it was found that end-heating was very effective in prolonging the runtime of the battery by reducing the heat-sink from the battery stack into the end insulation, and the effective initiation length of the heat paper fuse strip was a major factor in determining the overall rise time of the battery due to the much lower speed of flame propagation in the heat paper than in the NanoFoil.

15. SUBJECT TERMS
Thermal battery, thin film, NanoFoil, heat source, prototype, discharge, initiation

16. SECURITY CLASSIFICATION OF:			17. LIMITATION OF ABSTRACT	18. NUMBER OF PAGES	19a. NAME OF RESPONSIBLE PERSON
a. REPORT	b. ABSTRACT	c. THIS PAGE			Michael S. Ding
Unclassified	Unclassified	Unclassified	UU	32	19b. TELEPHONE NUMBER (*Include area code*) (301) 394-0249

Contents

List of Figures iv

List of Tables v

Acknowledgment vi

1. Introduction 1

2. Experimental 2

2.1 Materials 2

2.2 Determination of Discharge Characteristics and Rise Time of Battery Stacks and Devices 3

2.3 Determination of Temperature Profiles of Battery Stacks 4

2.4 Measurement and Regulation of Skin Temperatures on NanoFoil Components 4

2.5 Mitigation of Heat-Sink from Stack into End Insulation 4

2.6 Screening Thermal Cell Components and Down-Selection of the Prototype Composition 5

2.7 Gas Analysis of a NanoFoil-Heated Thin-Film Thermal Battery Stack 5

2.8 Prototyping a NanoFoil-Heated Thin-Film Thermal Battery 6

3. Results and Discussion 8

3.1 Regulation of Skin Temperatures on NanoFoil by Buffer Layers 8

3.2 Heat-Sink Effects and Their Mitigation 9

3.3 Gases Generated by a 12-Cell NanoFoil-Heated Thin-Film Thermal Battery Stack 12

3.4 Performance of NanoFoil-Heated Thin-Film Thermal Battery Stacks 13

3.4.1 Screening of Thermal Cell Components for the Best Combination 13

3.4.2 Effects of Effective Fuse Strip Length on Rise Time 14

3.4.3 Selected 12-Cell NanoFoil-Heated Thin-Film Thermal Battery Stacks 15

3.5 A NanoFoil-Heated Thin-Film Thermal Battery Prototype 19

4. Conclusions 22

5. References 23

Distribution List 24

List of Figures

Figure 1. A schematic for the discharge setup and the electrical and thermal characterization of a 2-cell NanoFoil-heated thin-film thermal battery stack. 3

Figure 2. A schematic for the experimental setup for the determination of peak temperature on the outer surface of the stainless steel buffer discs (in gray) sandwiching the NanoFoil disc (in yellow). Two Microtherm discs (in dark gray) bracketed the sandwich to prevent excessive heat loss through the ends. 4

Figure 3. A schematic demonstrating the measure taken to mitigate the heat-sink effects from the battery stack into the end insulation by adding a NanoFoil disc as compensating heat source on the outside of each of the electrodes (compared to figure 1). 5

Figure 4. Photos of the test fixture within which a 12-cell NanoFoil-heated thin-film thermal battery stack was sealed, initiated, and discharged while the pressure developed inside was recorded and gases collected and analyzed. 6

Figure 5. Photos of the 12-cell NanoFoil-heated thin-film thermal battery prototype at its various stages of construction. Top left: the 12-cell stack aligned and under a compression of 100 lb. before fuse strip attachment and wrapping; Top right: the 12-cell stack all wrapped up and ready to be connected to the header and sealed into its case; Bottom left: the steel header and can to encase the 12-cell stack; Bottom right, the final 12-cell NanoFoil-heated thin-film thermal battery prototype, consisting as the core the 12-cell NanoFoil-heated thin-film thermal battery stack and as the case the steel header and can laser welded to a hermetic seal. 8

Figure 6. Temperature-time curves developed on the outer surface of the buffer- NanoFoil-buffer sandwich after the NanoFoil was initiated, with buffer layers of different thicknesses as indicated in the plot. 9

Figure 7. Variation with buffer layer thickness of peak temperature developed on the outer surface of the buffer-NanoFoil-buffer sandwich, as determined from the temperature-time curves of figure 6. 9

Figure 8. Comparison of voltage-time (top plot) and resistance-time (bottom plot) curves for two 12-cell NanoFoil-heated thin-film thermal battery stacks, one with end-heating and one without, as differentiated by the legends in the plots. 10

Figure 9. Comparison of rise times for two 12-cell NanoFoil-heated thin-film thermal battery stacks, one with end-heating and one without, as differentiated by the legends. The rise time value is determined as the difference between the time the battery voltage becomes stable under the load and the time the power is supplied to the match wire. 11

Figure 10. Comparison of voltage-time (top plot) and resistance- and temperature-time (bottom plot) curves for two single-cell NanoFoil-heated thin-film thermal battery stacks, one with end-heating and one without, as differentiated by the legends in the plots. 12

Figure 11. Some results of screen tests on single-cell NanoFoil-heated thin-film thermal battery stacks in search of best combination for the prototype battery. The down-selected composition is indicated in the plots. 14

Figure 12. Voltage and temperature curves vs. time in the early part of discharge after initiation, demonstrating the effect of effective initiation length of the fuse strip on the overall rise time of the stack. 15

Figure 13. Discharge performance (top plot) of the first 12-cell NanoFoil-heated thin-film thermal battery stack and its temperature- and resistance-time curves (bottom plot). 16

Figure 14. Changes with time in voltages and temperatures for the first 12-cell NanoFoil-heated thin-film thermal battery stack. 17

Figure 15. Discharge performance (top plot) of the 12-cell NanoFoil-heated thin-film thermal battery stack with silicone rubber discs at one end for the maintenance of stack pressure and its temperature- and resistance-time curves (bottom plot). 18

Figure 16. Changes with time in voltage and temperature for the 12-cell NanoFoil-heated thin-film thermal battery with silicone rubber discs at one end for the maintenance of stack pressure. 19

Figure 17. Discharge performance (top plot) of the prototype NanoFoil-heated thin-film thermal battery device and its stack resistance-time curve (bottom plot). 20

Figure 18. Changes of voltages with time as measured on the match wire leads and the battery terminal leads for the prototype NanoFoil-heated thin-film thermal battery device. 21

Figure 19. Improvement in rise time of the prototype NanoFoil-heated thin-film thermal battery device over a traditional pressed-pellet thermal battery and NanoFoil-heated pressed-pellet thermal battery. 21

List of Tables

Table 1. Stack configuration for the prototype battery. 7

Table 2. Gases generated by a 12-cell NanoFoil-heated thin-film thermal battery stack 13

Acknowledgment

We thank the Office of the Secretary of Defense and the Joint Department of Defense (DOD)/Department of Energy (DOE) Munitions Technology Development Program for their financial and programmatic support, and Mr. Chris Janow in particular for his vision, efforts, and encouragement in the formulation, setup, and management of this program. We thank the Advanced Power Sources Group of Sandia National Laboratories for their collaboration in this program and the quality materials and components they supplied to us. We also thank many people at the U.S. Army Armament Research, Development, and Engineering Center for their support and collaborations, both past and present, which have helped the inception and growth of this program.

1. Introduction

Modern munitions require an increasing amount of onboard power and energy for enhanced functionality with diminishing volume and mass that can be allocated for the provision of such power and energy. This requirement poses a serious challenge to traditional thermal batteries, which have been one of the dominant means of meeting that requirement for the past half century (*1, 2*). Current traditional thermal batteries are based on pressed pellet technology, being manufactured by cold pressing electrochemical and pyrotechnic powders into pellets and then assembling these pellets into a thermal battery stack, which is then sealed in a steel can with proper insulation. This technology allows only incremental improvements in term of volume, mass, and energy/power density, and does not provide packaging flexibility. The next generation of thermal battery technology centers around the thin-film approach, which would allow for the fabrication of much thinner and flexible battery components that can be cut and conformed to a wide variety of shapes. It also promises thin-film thermal battery devices with a faster rise, higher power, and smaller volume.

To develop thin-film thermal battery technology, cathodes, anodes, and electrolytes in the form of coated films on substrates have been developed, and electrochemical cells made of these films cut to the desired shapes have been tested. But to build complete, fully functional thin-film thermal battery devices, a compatible new heat source is required with drastically different traits from those of traditional pyrotechnic pressed heat pellets. One answer to this requirement is the adapted application of NanoFoil® (*3, 4*), a trademarked metal foil made of alternating layers of aluminum and nickel, each with thickness typically of 100 nm or less (*5, 6*). This foil material has been shown to possess many inherent advantages as a new heat source material for thermal batteries, especially for thin-film thermal batteries. These advantages include rapid propagation of reaction front, fast heat delivery, flexible form factor, mechanical integrity, inherent conduction of electricity, and safety against accidental initiation. It also presents many new technical challenges, such as reliable initiation, control of peak skin temperature, reduction of stack resistance, and thermal insulation and management (*7–9*). This work aims at developing techniques and measures for realizing the potentials of the NanoFoil material as the new heat source for thin-film thermal batteries and overcoming its inherent technical barriers, with the ultimate goal of building a complete, fully functional NanoFoil-heated thin-film thermal battery prototype.

The work described here has been carried out under a program titled “NanoFoil-Heated Thin-Film Thermal Battery” set up and funded by the Joint Department of Defense (DOD)/Department of Energy (DOE) Munitions Technology Development Program (JMP) under the direction of the Office of the Secretary of Defense (OSD). It was also leveraged by a few Army Technology Objectives (ATOs) and Technology Program Annexes (TPAs) by the

Armament Research, Development, and Engineering Center (ARDEC) and U.S. Army Research Laboratory (ARL). The lead of this program is the Munitions Battery Team of ARL, and the major technical partner is the Advanced Power Sources Group of Sandia National Laboratories (SNL). The latter group has been developing thin-film technologies for making thin-film cathodes, anodes, and electrolytes of thermal batteries for many years, and has been responsible for making and supplying those components, with adjustments and improvements when necessary, to the ARL team, which has been charged with building, initiating, and testing the cathode, anode, and electrolyte components with NanoFoil as the exclusive heat source for the program. The ARL team is also leading the efforts for optimizing the different components for multi-cell stacks and for ultimately designing, building, and characterizing prototype NanoFoil-heated thin-film thermal batteries as deliverables for the program. The use of NanoFoil as the heat source alternative to the traditional pyrotechnic pressed pellets for thermal batteries was pioneered by the same ARL team and an ARDEC team in 2007 (*8, 9*). This technology was subsequently developed and matured to the point that it could be reliably and profitably employed in a variety of thermal battery settings. The JMP-OSD program "NanoFoil-Heated Thin-Film Thermal Battery" was set up to compatibilize, merge, and synergize the NanoFoil technology and the thin-film technology for thermal batteries to develop and prototype a NanoFoil-heated thin-film thermal battery for those applications that require a power source with fast rise, small volume, irregular form factor, high voltage, or high power. It was also hoped that the combination of thin-film and NanoFoil technologies would eventually lead to continuous production of thermal batteries, as opposed to the traditional batch mode, with higher production efficiency, greater materials utilization, and lower cost.

2. Experimental

2.1 Materials

NanoFoil discs for this work were custom-made by Indium Corporation according to our specification from a braze-free, sputtered aluminum (Al)-nickel (Ni) NanoFoil of 150 μm thickness, cut into 0.75-in-diameter discs with a special die. The delivered NanoFoil discs had an average weight of 0.22 g per disc, a reasonably smooth edge, somewhat limited flexibility, and metallic silver color.

Thin-film components of anode/electrolyte and cathode were prepared by a coating method at SNL. These coated sheets, ranging from 5 to 11 mils in thickness, were cut with a precision die into discs of 0.75 in diameter. The assemblage and testing of the NanoFoil-heated thin-film thermal battery stacks from the above components was carried out at ARL, in a dry room with a typical dew point of –56 °C (0.074% relative humidity).

Figure 1 depicts a typical experimental setup for an assembled NanoFoil-heated thin-film thermal battery stack (2-cell). The stack was compressed with typically 100-lb force and fixed between a pair of stainless steel cylinders on a mechanical press. For initiation of the NanoFoil discs in the stack, a piece of heat paper, about 0.25-inch in width and stack-height in length, was wrapped against the side of the stack with a piece of glass tape. For those tests that could be carried out on a stack right there on the mechanical press, a nichrome wire fixed in space was made in touch with a portion of exposed fuse strip for initiation. For those that required relocation of the stack into a fixture or a battery case, a nichrome wire was pressed against the top portion of the fuse strip with a Microtherm disc.

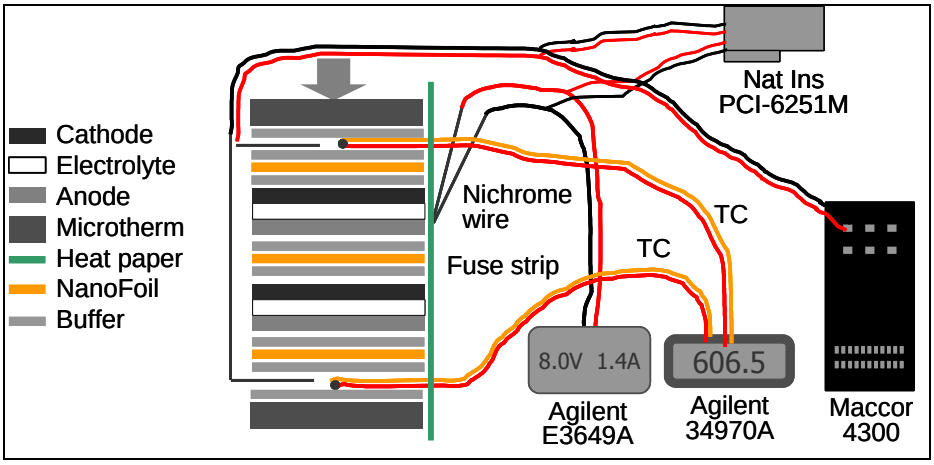

Figure 1. A schematic for the discharge setup and the electrical and thermal characterization of a 2-cell NanoFoil-heated thin-film thermal battery stack.

2.2 Determination of Discharge Characteristics and Rise Time of Battery Stacks and Devices

Figure 1 depicts the experimental setup for a 2-cell NanoFoil-heated thin-film battery stack, its initiation, its discharge, and the monitoring and recording of its rise time and temperature. The rise time value is determined as the difference between the time the battery voltage becomes stable under the load and the time the power is supplied to the match wire. For temperature recording, although figure 1 depicts a situation where the temperatures were recorded with an Agilent data logger, they were some times recorded with the NI PCI-6251M high-speed data acquisition system when a high sampling rate was desirable. The power for the initiation was generated with a DC power supply limited at 1.4 A and 8 V. Electrical discharge and testing was done with a Maccor 4300 system, with a discharge schedule of a constant current, typically 142 mA, superimposed with a –42-mA, 10-ms current pulse every second. The current pulse was applied so that the internal resistance of the battery could be calculated from the current pulse and the voltage response. The voltage changes on the match wires, the battery terminals, and the thermocouple terminals were measured and recorded with a high-speed data acquisition system at the sampling rate of 10,000 S/s.

2.3 Determination of Temperature Profiles of Battery Stacks

Also shown in figure 1 is the sub-system of temperature measurement and logging for the battery stack under test. The actual spots where such temperature values were collected were on the two electrodes made of 3-mil-thick stainless steel discs. For this, a K-type thermocouple tip was made out of 0.020-mil wires with an Omega thermocouple welder, which was then flattened with a mechanical press and spot-welded onto an electrode with a Miyachi Unitek resistance welder. On the same electrode were then spot-welded the current and sense leads for the battery stack discharge. The measurement and recording of the temperatures was carried out with an Agilent data logger or with the same high-speed data acquisition system when such sampling rate was desired.

2.4 Measurement and Regulation of Skin Temperatures on NanoFoil Components

As magnesium metal foil was used for the anode material for the thin-film thermal cells, the peak temperature adjacent to the anode had to be limited to 650 °C to prevent its melting. For this reason, a series of work was carried out in which pairs of stainless steel buffer discs of different thicknesses were used to sandwich a NanoFoil disc of 150 μm thickness. The NanoFoil disc was then initiated, and the temperature-time curve on the outer surface of the upper buffer disc was measured and recorded. From this curve, a peak temperature was subsequently determined, which was repeated for a number of buffer layers with different thicknesses. Figure 2 shows the experimental setup.

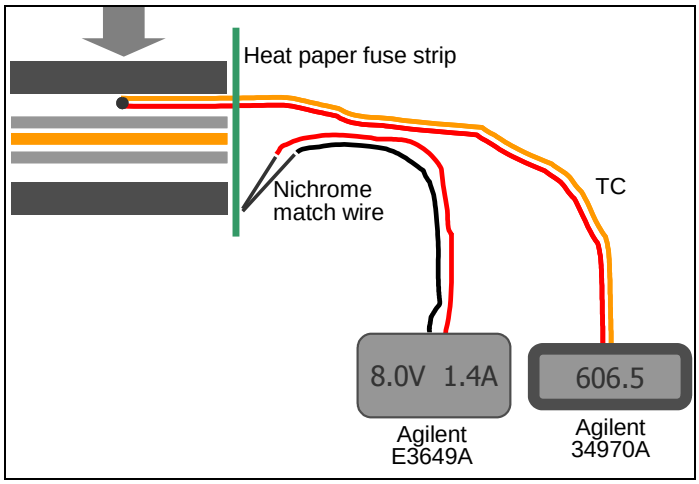

Figure 2. A schematic for the experimental setup for the determination of peak temperature on the outer surface of the stainless steel buffer discs (in gray) sandwiching the NanoFoil disc (in yellow). Two Microtherm discs (in dark gray) bracketed the sandwich to prevent excessive heat loss through the ends.

2.5 Mitigation of Heat-Sink from Stack into End Insulation

To reduce the heat-sink from the stack into the ends of the end insulation materials, an extra buffer-NanoFoil-buffer sandwich was added to the outside of each of the electrodes after a

Microtherm disc, as depicted in figure 3 (compare to figure 2); however, the buffer layers here employed 2-mil-thick stainless steel discs instead of the 5-mil-thick discs used in all other buffer-NanoFoil-buffer heating stacks. The appropriateness of the 2-mil thickness for the additional end buffer was found out by experimenting with single-cell NanoFoil-heated thin-film thermal battery stacks.

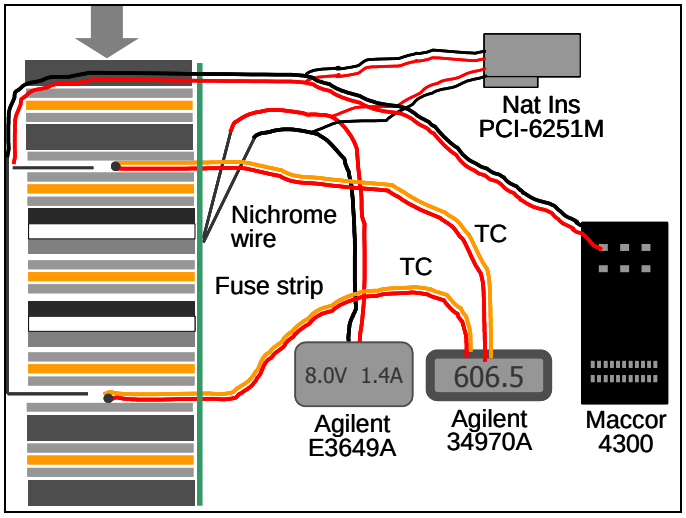

Figure 3. A schematic demonstrating the measure taken to mitigate the heat-sink effects from the battery stack into the end insulation by adding a NanoFoil disc as compensating heat source on the outside of each of the electrodes (compared to figure 1).

2.6 Screening Thermal Cell Components and Down-Selection of the Prototype Composition

One of the first experimental goals for the program was to determine the best combination of cathode, anode, electrolyte, and NanoFoil in terms of their chemical compositions, physical properties, and material treatment histories. Out of the many varieties of cathode and anode/electrolyte components produced and supplied by SNL and the two kinds of NanoFoil discs of thicknesses 150 and 80 μm we had available to us, we tested an array of single-cell NanoFoil-heated thermal battery stacks, in a testing setup depicted in figure 1. The use of 80-μm NanoFoil was soon rejected because of its insufficient heat content for the thin-film thermal battery components tested. Through a series of experiments with the 150-μm NanoFoil discs as the exclusive heat source, we eventually identified the optimal combination of cathode, anode/electrolyte, NanoFoil, and buffer components for constructing the prototype NanoFoil-heated thin-film thermal batteries.

2.7 Gas Analysis of a NanoFoil-Heated Thin-Film Thermal Battery Stack

Collection of gases generated by a 12-cell NanoFoil-heated thin-film thermal battery stack was carried out in a test fixture shown in figure 4. The hermetic seal was achieved by using silicone gaskets between the fixture cover and body for passing the match wire leads and battery leads

from inside the fixture to the outside, as can be seen in the bottom photo of figure 4. A copper tube was then connected to the connecting port (shown in the top photo), the other end of which was connected to a manifold for fixture evacuation, gas collection, and pressure monitor. After evacuating the fixture, the battery stack was initiated and gas samples were collected at different times, which were subsequently removed and analyzed using gas chromatography (*10, 11*).

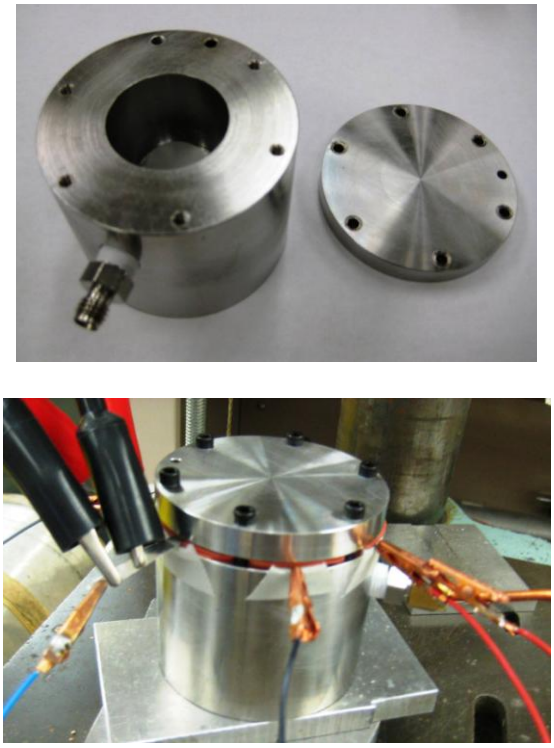

Figure 4. Photos of the test fixture within which a 12-cell NanoFoil-heated thin-film thermal battery stack was sealed, initiated, and discharged while the pressure developed inside was recorded and gases collected and analyzed.

2.8 Prototyping a NanoFoil-Heated Thin-Film Thermal Battery

The making of the prototype NanoFoil-heated thin-film thermal battery proceeded according to the following procedure (see table 1 and figure 5). The electrode was made from 3-mil-thick, 0.75-in-diameter stainless steel disc by spot-welding to it a strip of stainless steel of same thickness as the electrode lead. On the side facing the stack, the electrode lead was covered with a wider strip of mica, which was fixed to the lead with glue glass tape, to prevent the electrode lead from getting shorted by extruded molten electrolyte (upper-right photo of figure 5). These two electrodes were then aligned with the other stack components into a stack according to the sequence indicated in table 1. After attaching a match wire with a piece of heat paper at the top of the stack, another piece of Microtherm disc was placed on top, and the whole stack was then transferred to a mechanical press and compressed with a pressure of about 100 lb, as shown in the upper-left photo of figure 5. A piece of heat paper about 0.25 in wide and about stack-height

long was then attached to the side of the stack with a piece of glass tape, the upper end of the fuse strip in firm contact with the piece of heat paper in touch with the match wire. The whole stack was then wrapped tightly with about 10 layers of glass tape for thermal insulation and mechanical stability, as shown in the upper-right photo of figure 5. The pair of battery electrode leads and the pair of match leads were then connected to the properly designated posts on the header by spot-welding (see the lower-left photo of figure 5). The battery stack was then lowered into the battery can, the header was pushed into the can until the tops of the header and the rim of the can were flush, and the case was hermetically sealed with a Miyachi Unitek laser welder, as shown in the lower-right photo of figure 5.

Table 1. Stack configuration for the prototype battery.

Layer	Materials	Thickness /mil
Thermal insulation	Microtherm	90 (uncompressed)
Match wire	Nichrome	
Thermal insulation	Microtherm	90 (uncompressed)
Heat source	NanoFoil	150 μm
Heat buffer	Stainless steel	2
Thermal insulation	Microtherm	90 (uncompressed)
Positive electrode	Stainless steel	3
Heat buffer	Stainless steel	5
Heat source	NanoFoil	150 μm
Heat buffer	Stainless steel	5
Cathode substrate	Not listed	Not listed
Cathode	Not listed	Not listed
Separator	Not listed	Not listed
Anode/substrate	Not listed	Not listed
Heat buffer	Stainless steel	5
Heat source	NanoFoil	150 μm
Heat buffer	Stainless steel	5
Negative electrode	Stainless steel	3
Thermal insulation	Microtherm	90 (uncompressed)
Heat buffer	Stainless steel	2
Heat source	NanoFoil	150 μm
Heat buffer	Stainless steel	2
Thermal insulation	Microtherm	90 (uncompressed)

Notes: All components are of 0.75 in diameter and layers colored blue are repeated 12 times.

Figure 5. Photos of the 12-cell NanoFoil-heated thin-film thermal battery prototype at its various stages of construction. Top left: the 12-cell stack aligned and under a compression of 100 lb before fuse strip attachment and wrapping. Top right: the 12-cell stack all wrapped up and ready to be connected to the header and sealed into its case. Bottom left: the steel header and can to encase the 12-cell stack. Bottom right: the final 12-cell NanoFoil-heated thin-film thermal battery prototype, consisting as the core the 12-cell NanoFoil-heated thin-film thermal battery stack and as the case the steel header and can laser welded to a hermetic seal.

3. Results and Discussion

3.1 Regulation of Skin Temperatures on NanoFoil by Buffer Layers

As magnesium metal foil was used for the anode material for the thin-film thermal cells, the peak temperature adjacent to the anode had to be limited to 650 °C to prevent its melting. For this reason, a series of work was carried out in which pairs of stainless steel buffer discs of different thicknesses were used to sandwich a NanoFoil disc of 150 μm thickness. The NanoFoil disc was then initiated, and the peak temperature on the outer surface of the buffer discs was subsequently measured. The results are plotted in figures 6 and 7, from which it can be seen that a pair of buffer discs with a minimum thickness of 5 mils were needed for a NanoFoil disc of 150 μm thickness to prevent anode from melting.

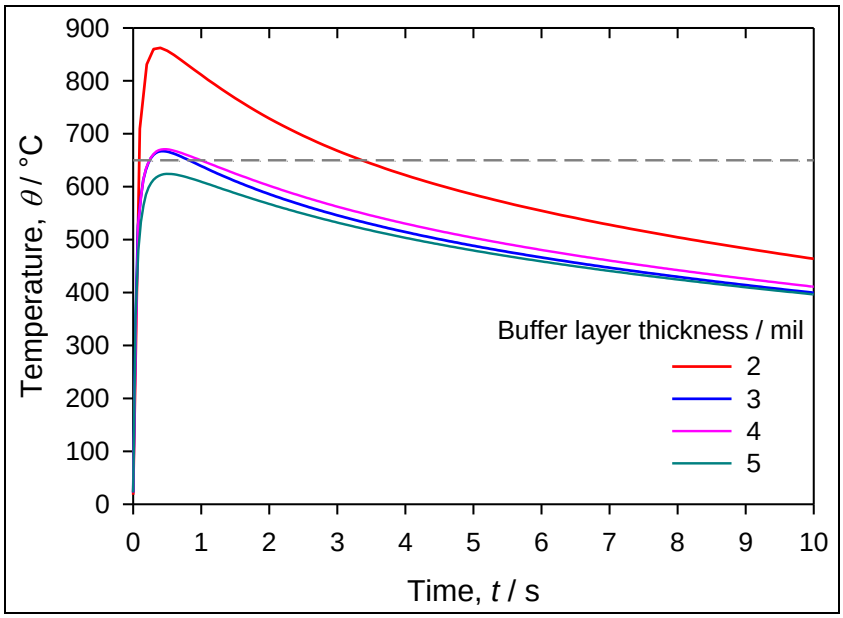

Figure 6. Temperature-time curves developed on the outer surface of the buffer-NanoFoil-buffer sandwich after the NanoFoil was initiated, with buffer layers of different thicknesses as indicated in the plot.

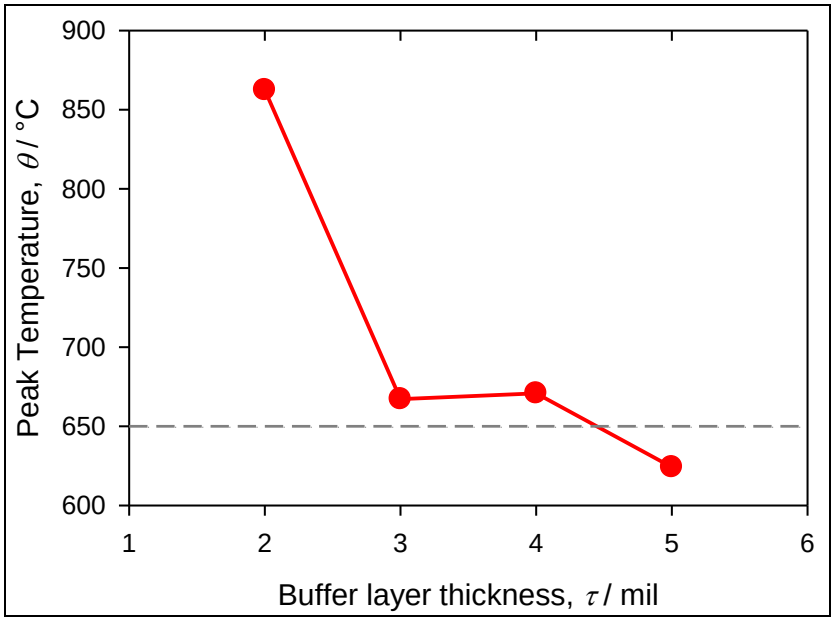

Figure 7. Variation with buffer layer thickness of peak temperature developed on the outer surface of the buffer-NanoFoil-buffer sandwich, as determined from the temperature-time curves of figure 6.

3.2 Heat-Sink Effects and Their Mitigation

As shown in figures 8 and 9, conditions of thermal insulation on the stack ends have pronounced effects on the performance of the battery stacks. This is mainly due to the geometric nature of the thin-film thermal battery stacks, which in most cases will have much higher values of diameter-

to-thickness ratio than the conventional pressed-pellet thermal battery stacks. As shown in figure 8 (top plot), provision of end-heating by the addition of one more NanoFoil heating stack to each end of the 12-cell NanoFoil-heated thin-film thermal battery stack (see figure 3) prolonged the runtime of the stack to about 50 s from 30 s for a similar stack without the end-heating. The bottom plot of figure 8 plots stack resistance values calculated from the current-voltage pulses in the top-plot curves, which shows the two stacks to have similar stack resistances in their respective operation ranges.

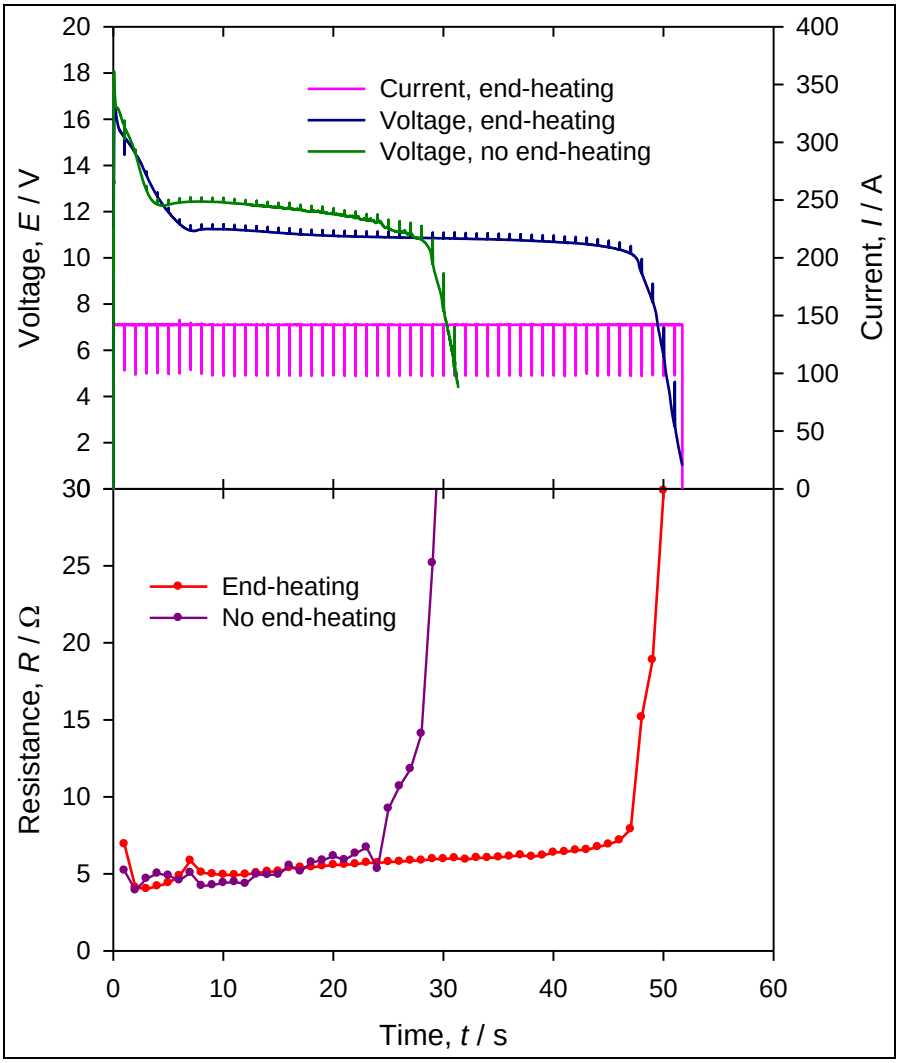

Figure 8. Comparison of voltage-time (top plot) and resistance-time (bottom plot) curves for two 12-cell NanoFoil-heated thin-film thermal battery stacks, one with end-heating and one without, as differentiated by the legends in the plots.

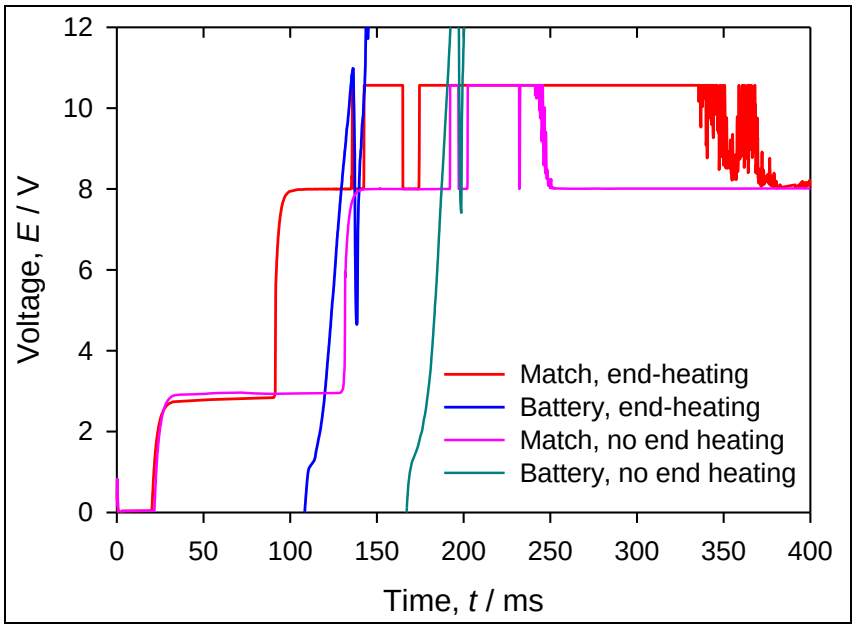

Figure 9. Comparison of rise times for two 12-cell NanoFoil-heated thin-film thermal battery stacks, one with end-heating and one without, as differentiated by the legends. The rise time value is determined as the difference between the time the battery voltage becomes stable under the load and the time the power is supplied to the match wire.

According to figure 9, the provision of end-heating not only prolonged the runtime of the 12-cell stack but also shortened the rise time significantly. However, the correlation here is not immediately clear, as the time in which the rise time phenomenon takes effect is much shorter than that for the end-heating to take effect. It is however possible that the provision of end-heating improved the uniformity of the initiation of NanoFoil discs between the ends, thus indirectly enabling the stack to come up faster in voltage.

The effects to prolong the runtime by end-heating are more dramatic in the single-cell stack setting, which is entirely within expectation as the single-cell stacks have even higher values of diameter-to-thickness ratio than the 12-cell stacks. This is clearly demonstrated in figure 10, which shows a prolonging of runtime from 10 to 45 s by the provision of end-heating to a single-cell stack.

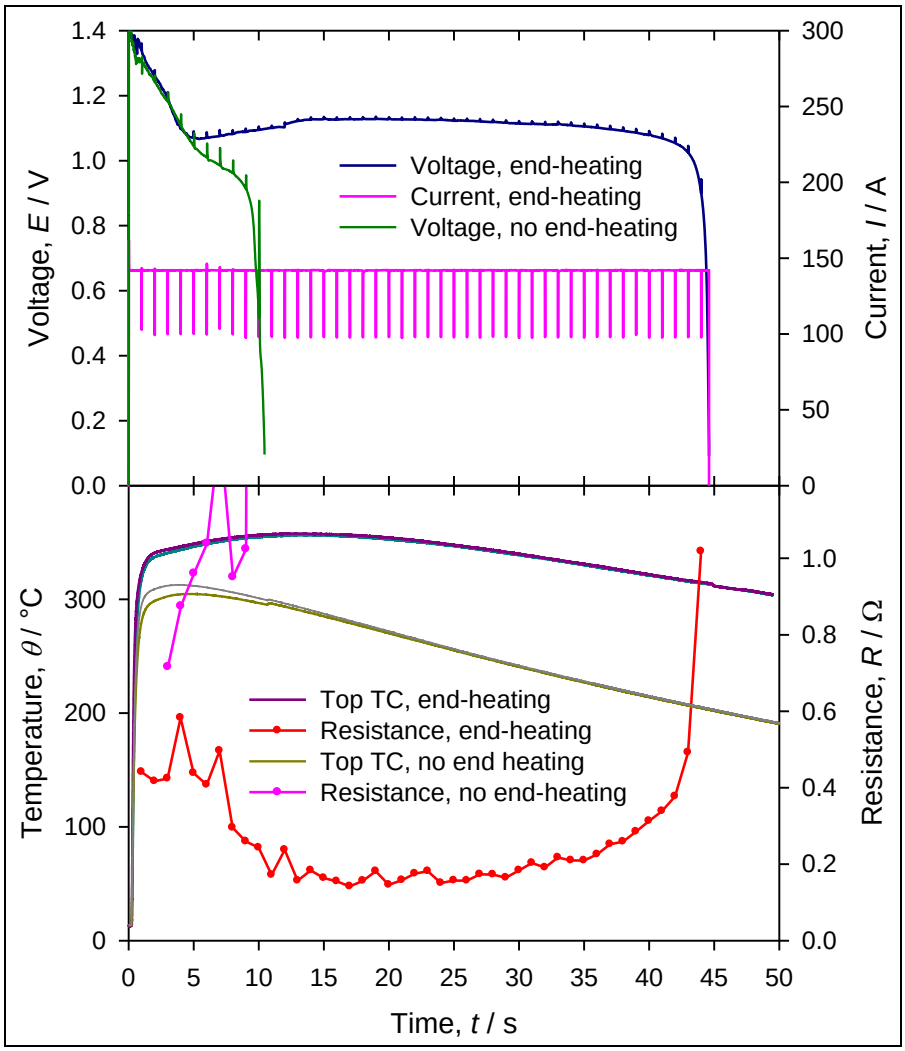

Figure 10. Comparison of voltage-time (top plot) and resistance- and temperature-time (bottom plot) curves for two single-cell NanoFoil-heated thin-film thermal battery stacks, one with end-heating and one without, as differentiated by the legends in the plots.

3.3 Gases Generated by a 12-Cell NanoFoil-Heated Thin-Film Thermal Battery Stack

Gases generated inside the case of a thermal battery are known to be detrimental to the operation of the thermal battery. Moderate amounts of generated gases, especially the lighter components such as H_2, contribute to the heat conduction from stack core to the case, thus shortening the runtime of the battery. Higher amounts would generate excessive pressure to deform or bulge the case. Excessively high amounts would even rupture a glass-to-metal seal around an electrode and cause the battery to vent, thus creating a hazardous situation.

The gases generated by a 12-cell NanoFoil-heated thin-film thermal battery stack were less than moderate. As shown in table 2 for the results of gas analysis for the stack, the total pressure inside the fixture was around 100 Torr, which is much lower than that inside thin-film thermal

batteries of other technologies, even lower than that inside a typical traditional pressed-pellet thermal battery. This low pressure of gas is not expected to contribute greatly to the heat loss mechanisms of the thermal battery, even though the main component of the generated gas was H_2 according to the analysis. Furthermore, this low pressure is reflected in the completely un-deformed, un-bulged battery case after the initiation and discharge of the battery, as was visually observed.

Table 2. Gases generated by a 12-cell NanoFoil-heated thin-film thermal battery stack.

Sample	Total Pressure / Torr	H_2	O_2	N_2	CO	CH_4	CO_2
First	100.7	80.6	0.0	0.0	17.2	2.2	0.0
Second	100.2	68.6	6.8	6.3	14.0	4.3	0.0

3.4 Performance of NanoFoil-Heated Thin-Film Thermal Battery Stacks

3.4.1 Screening of Thermal Cell Components for the Best Combination

One of the first set of experiments to have been carried out here at ARL was to systematically screen the many kinds of cathode and anode/electrolyte with different chemical compositions and different treatment and production histories for the most compatible combination with the NanoFoil heat source for the production of a NanoFoil-heated thin-film thermal battery prototype. Such screening took the form of building, initiating, and testing many single-cell NanoFoil-heated thin-film thermal battery stacks, which resulted in many discharge and rise time curves. Out of the multitude of curves, a selected few are plotted in figure 11 to provide an indication of what was typically observed and what kinds of data were typically gathered, processed, and analyzed. In particular, the set of curves is singled out in the plot corresponding to the combination down-selected from the screening for the subsequent prototyping for the NanoFoil-heated thin-film thermal battery.

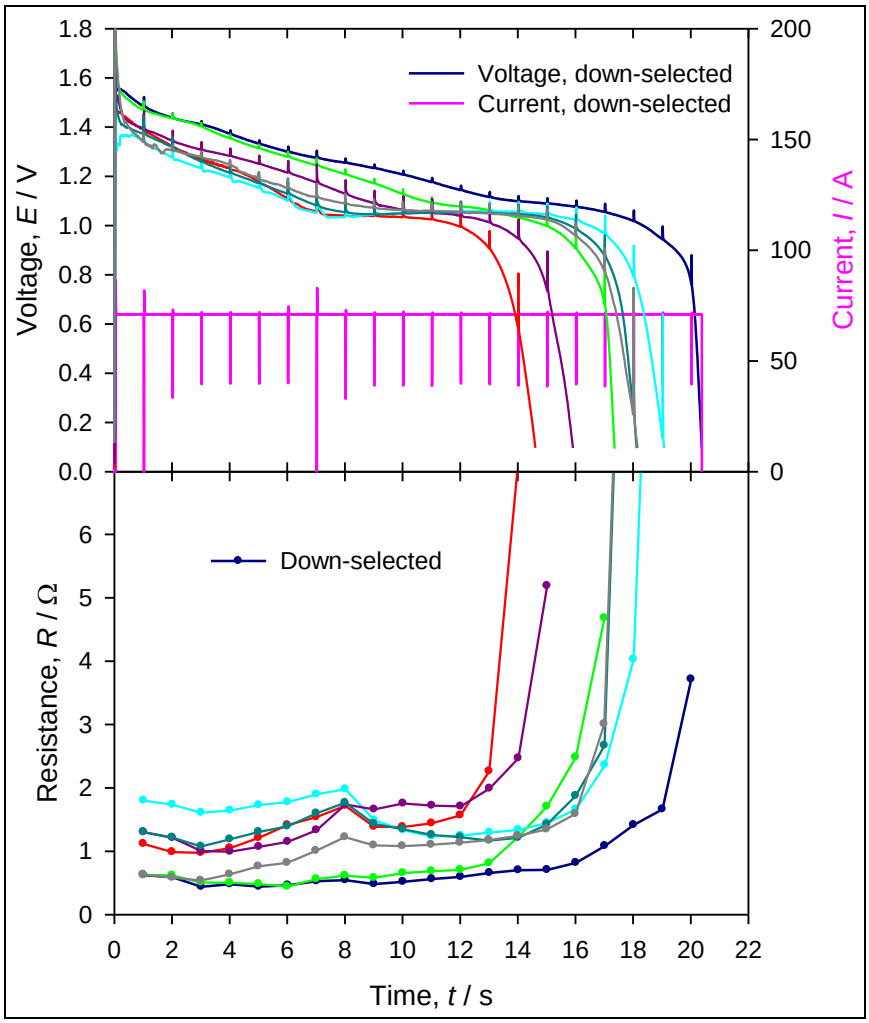

Figure 11. Some results of screen tests on single-cell NanoFoil-heated thin-film thermal battery stacks in search of best combination for the prototype battery. The down-selected composition is indicated in the plots.

3.4.2 Effects of Effective Fuse Strip Length on Rise Time

The speed of flame propagation along a piece of NanoFoil is about 9 m/s once initiated (*7*), while that along a piece of heat paper is on the order of 10 cm/s. It follows that in an initiation chain from the match wire to the heat paper fuse strip to the edge of the farthest NanoFoil discs to the whole of that disc, the length of the heat paper that effectively forms part of the initiation chain would be a dominant factor in determining the overall rise time of the NanoFoil-heated thin-film thermal battery stack. Such a situation is clearly demonstrated in one of the experiments executed on a series of single-cell NanoFoil-heated thin-film thermal battery stacks, of which the results are plotted in figure 12. As is shown, by positioning the match wire in the middle instead of the end of the fuse strip, the rise time of the stack was shortened from 220 to 150 ms. Their respective temperature curves show corresponding changes in time, consistent with the changes in battery stack voltages.

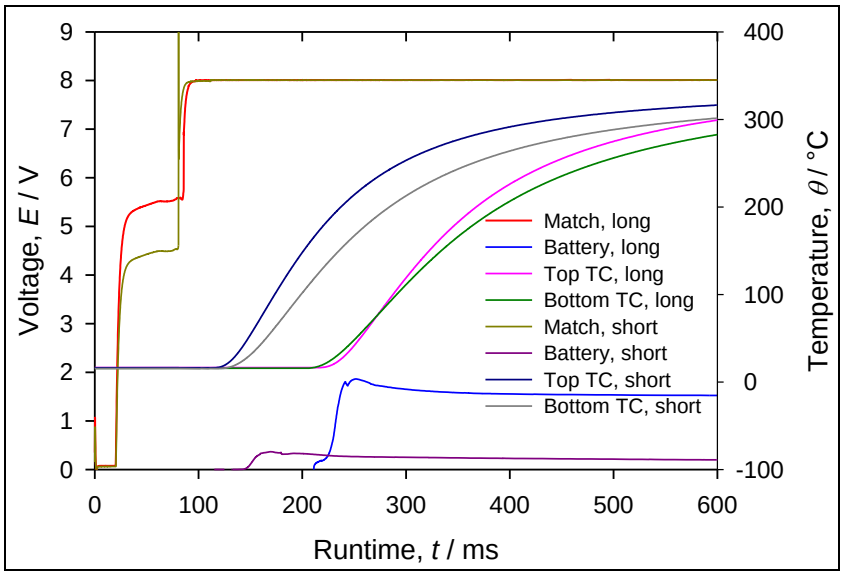

Figure 12. Voltage and temperature curves vs. time in the early part of discharge after initiation, demonstrating the effect of effective initiation length of the fuse strip on the overall rise time of the stack.

3.4.3 Selected 12-Cell NanoFoil-Heated Thin-Film Thermal Battery Stacks

The first 12-cell NanoFoil-heated thin-film thermal battery stack was built without end-heating. On discharge, the stack delivered about 43 s of service time under the current load of 142 mA (equivalent to 50 mA/cm^2), with a reasonably flat voltage plateau, as shown in the upper plot of figure 13. The stack resistance, as calculated from the voltage and current pulses placed in the discharge current profile specifically for this purpose, displayed reasonable values as plotted in the lower plot of figure 13. However, its rise time was unacceptably long, about 700 ms, as shown in figure 14, which is comparable to those of the traditional pressed-pellet thermal batteries. Upon closer inspection after plotting the temperature-time curves on the electrodes together with the voltage curves, shown in figure 14, it can be seen that the temperature on the bottom electrode was wavering and slow in rising, consistent with the slow rise in voltage on the battery. This is likely due to some uneven initiations of the NanoFoil discs in the stack.

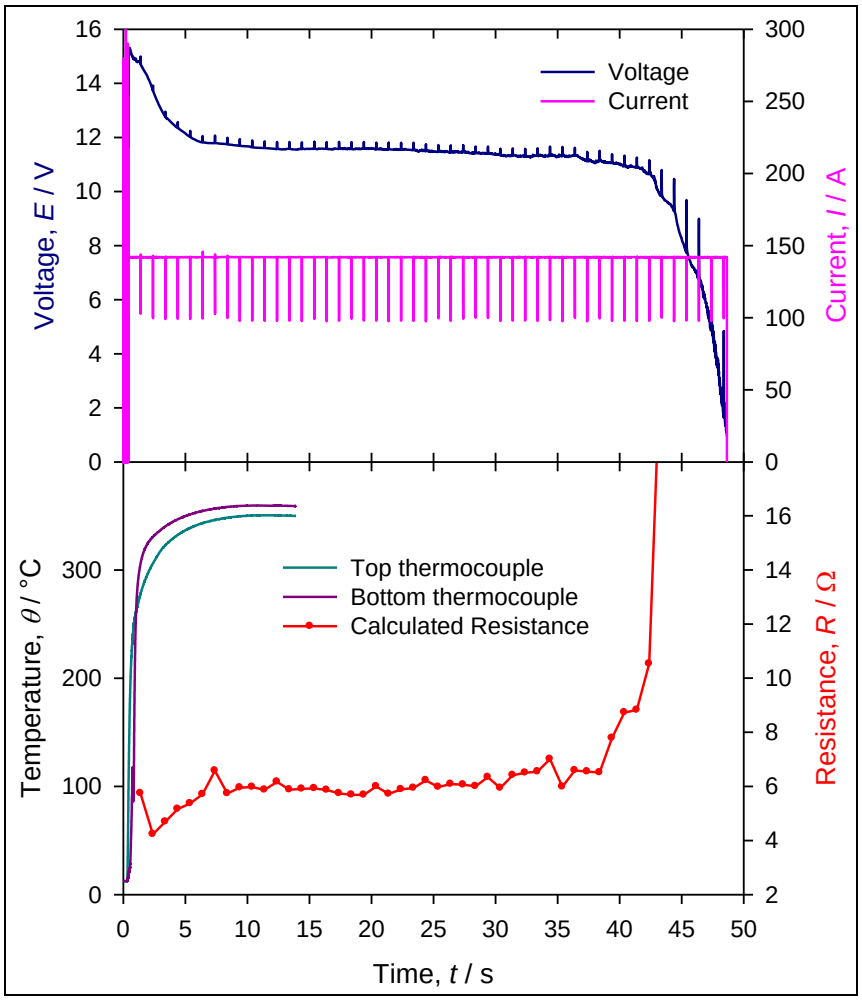

Figure 13. Discharge performance (top plot) of the first 12-cell NanoFoil-heated thin-film thermal battery stack and its temperature- and resistance-time curves (bottom plot).

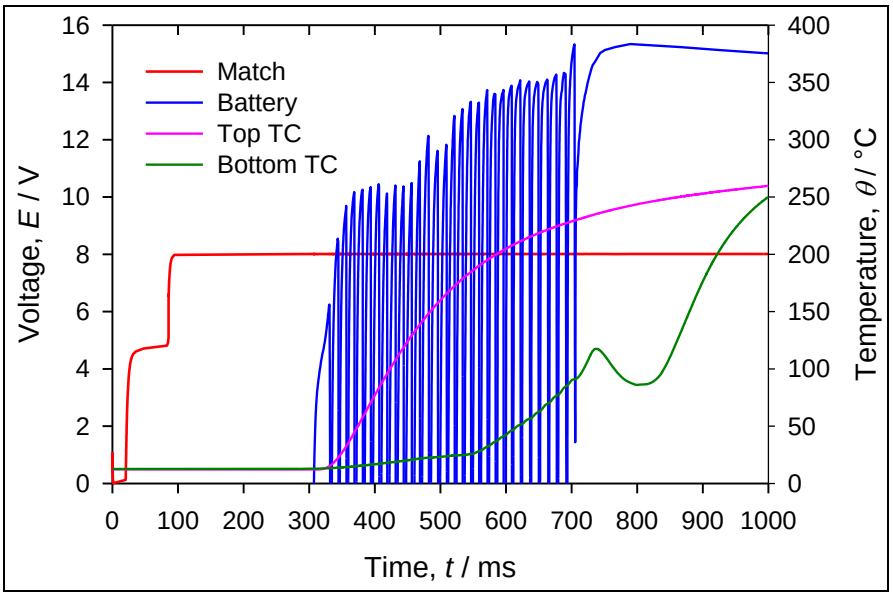

Figure 14. Changes with time in voltages and temperatures for the first 12-cell NanoFoil-heated thin-film thermal battery stack.

To reduce the stack resistance and thus enhance the power capability of the NanoFoil-heated thin-film thermal battery stack, silicon rubber discs were added to the ends on the outside of the stack in the hope that the elasticity of these discs would work to maintain the stack pressure upon initiation, which is typically accompanied by a significant drop in stack pressure due to the partial melting and relaxation of the components in the stack. The test results of such a rubber-cushioned 12-cell NanoFoil-heated thin-film stack are plot in figure 15, which shows in the lower plot a significant reduction in stack resistance in the early part of the discharge as compared to figure 13. But the performance of the stack started to deteriorate after about 20 s into the discharge, with a steady decline in voltage and rise in stack resistance. The rubber discs were later found to be severely deformed and charred. This method of using silicone rubber discs on the ends to maintain stack pressure was therefore deemed non-workable after this experiment, even though the rise time of the stack seemed to have improved also, as a comparison of figure 16 with figure 14 would show.

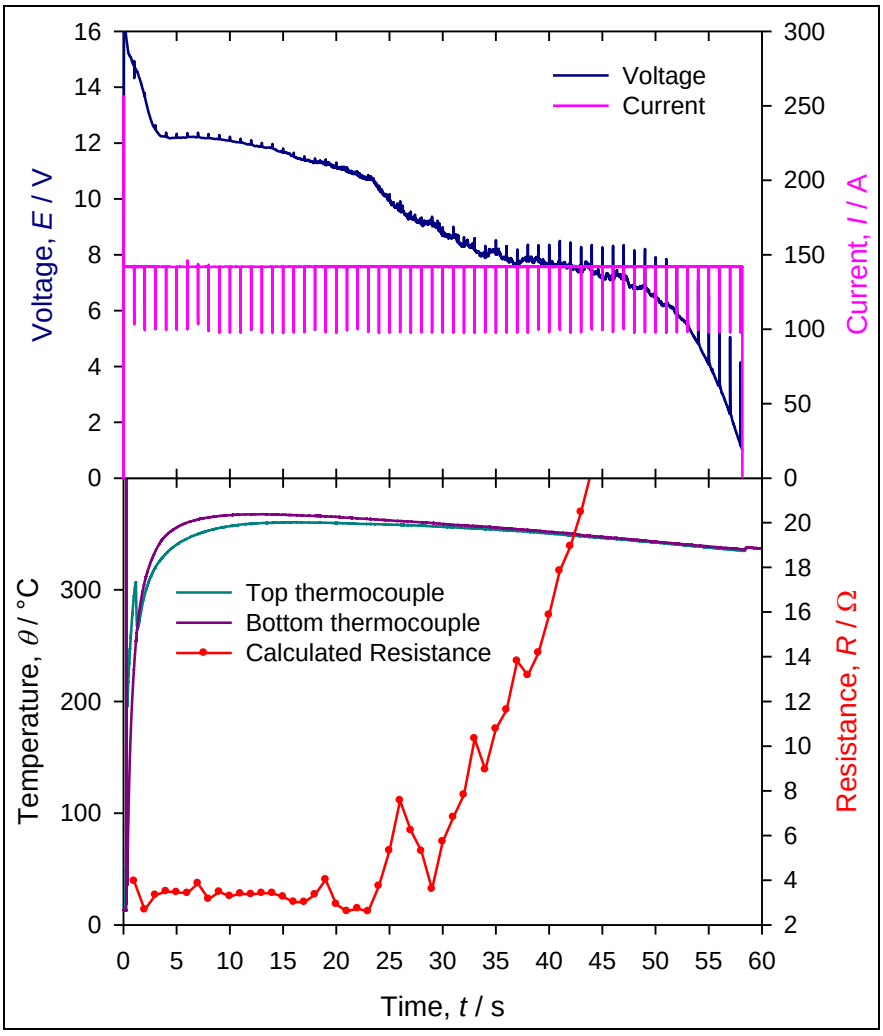

Figure 15. Discharge performance (top plot) of the 12-cell NanoFoil-heated thin-film thermal battery stack with silicone rubber discs at one end for the maintenance of stack pressure and its temperature- and resistance-time curves (bottom plot).

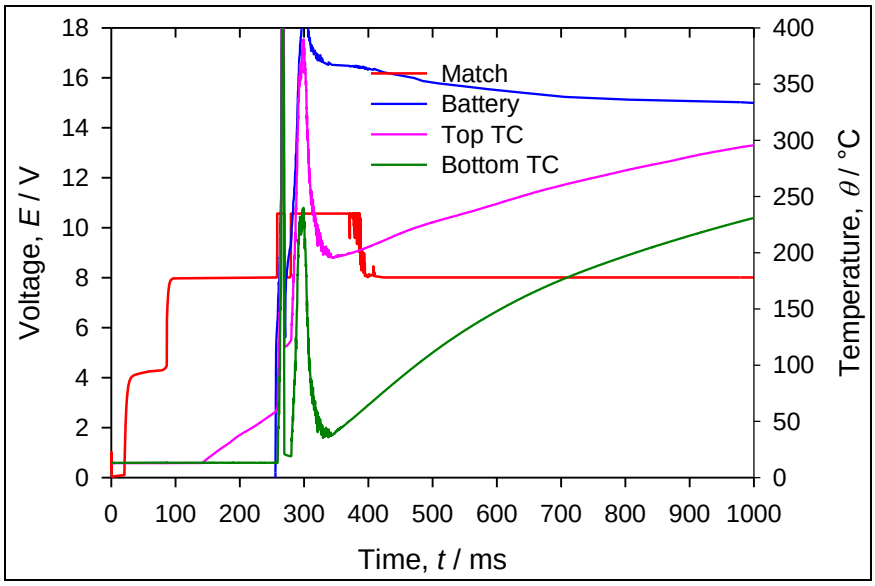

Figure 16. Changes with time in voltage and temperature for the 12-cell NanoFoil-heated thin-film thermal battery with silicone rubber discs at one end for the maintenance of stack pressure.

3.5 A NanoFoil-Heated Thin-Film Thermal Battery Prototype

All the efforts described in the preceding sections eventually led to the design and construction of a prototype 12-cell NanoFoil-heated thin-film thermal battery. The selection of the 12-cell design for the prototyping was a compromise between limiting the material cost of the prototype stacks and demonstrating the benefits of building multi-cell stacks with thin-film electrochemical components and NanoFoil as the heat source.

As plotted in figure 17, the prototype battery performed well under the current load of 142 mA (equivalent to 50 mA/cm^2). The runtime of 50 s was satisfactory considering the limited heat contents of the NanoFoil discs and the short-time nature of the targeted applications. The other discharge properties, such as stack resistance, voltage plateau, and the ability to carry the current load, were also good. The voltage-time curves of figure 18 give a rise time of about 140 ms, a significant improvement over the earlier 12-cell stacks and over other technologies. This can be clearly seen in figure 19, which plots together the rise time curves of the prototype battery with two other batteries, one with the pressed-pellets for the anode and cathode-electrolyte and a pyrotechnic heat source, and one with anode and cathode-electrolyte pellets and NanoFoil discs as the heat source.

The improvement in runtime and in initiation of the prototype battery over earlier 12-cell stacks can be seen by comparing figure 17 with figures 13 and 15, and by comparing figure 18 with figures 14 and 16.

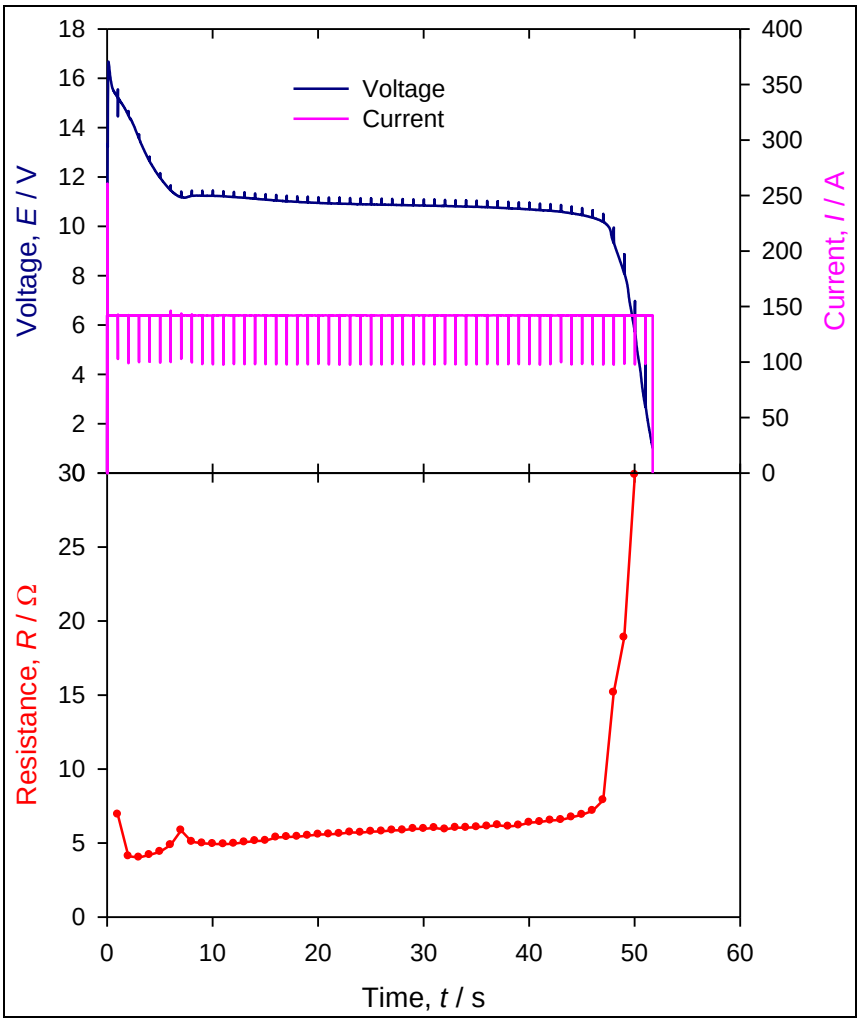

Figure 17. Discharge performance (top plot) of the prototype NanoFoil-heated thin-film thermal battery device and its stack resistance-time curve (bottom plot).

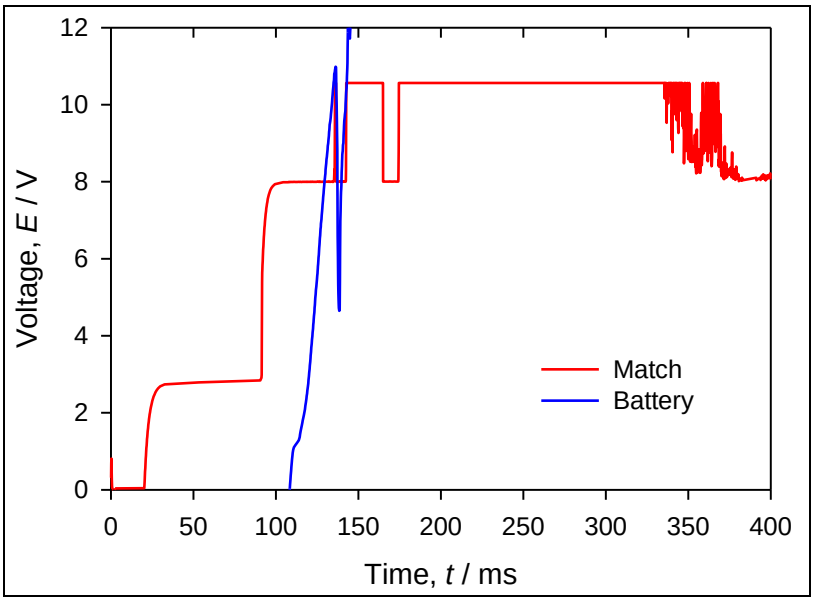

Figure 18. Changes of voltages with time as measured on the match wire leads and the battery terminal leads for the prototype NanoFoil-heated thin-film thermal battery device.

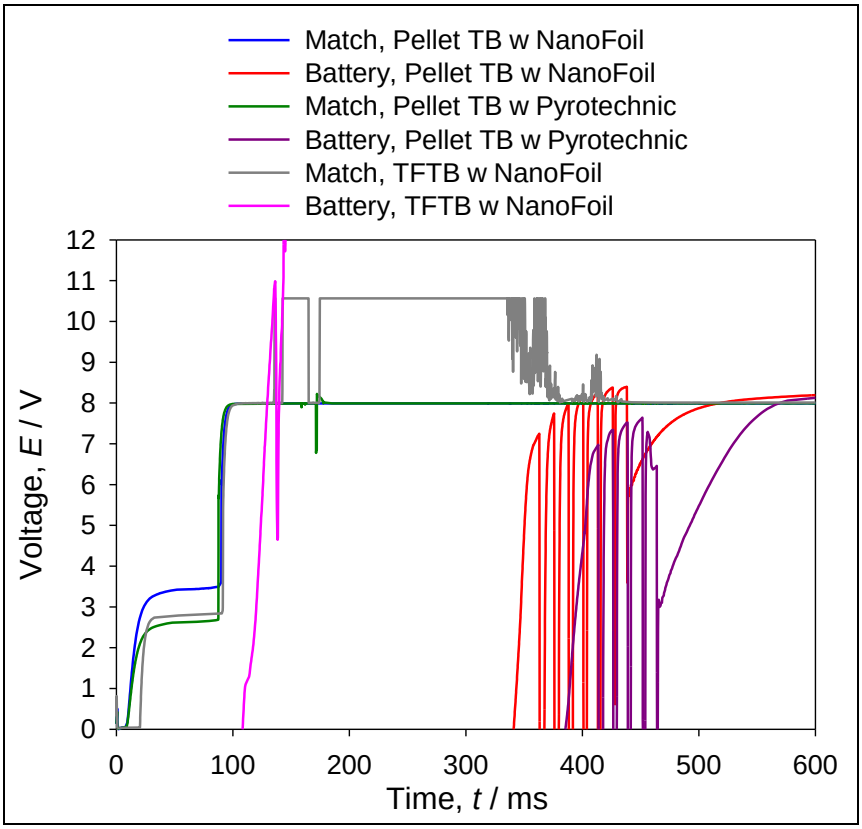

Figure 19. Improvement in rise time of the prototype NanoFoil-heated thin-film thermal battery device over a traditional pressed-pellet thermal battery and a NanoFoil-heated pressed-pellet thermal battery.

4. Conclusions

A 12-cell NanoFoil-heated thin-film thermal battery was prototyped for the first time, which upon initiation and discharge demonstrated good operational performance. The rise time of the prototype was 140 ms, a significant improvement over the earlier 12-cell stacks and over other technologies. The runtime of 50 s was reasonably long considering the limited heat contents of the NanoFoil discs and the short-time nature of the targeted applications. The other discharge performance properties were also satisfactory, such as stack resistance, voltage plateau, and the ability to carry the current load.

A number of factors in the design of the prototype were found to be critical for the performance of the battery device. End-heating was found to significantly prolong the runtime by efficiently reducing the heat-sink from the stack into the end insulation on account of the high diameter-to-thickness ratios of the thin-film thermal batteries. The position of the match wire on the heat paper fuse strip was found to be effective in affecting the overall rise time of the stack; the shorter length of the reaction path in the fuse strip invariably led to a shorter rise time, as the reaction propagation speed in the heat paper is about two orders of magnitude smaller than in the NanoFoil.

The gases generated by the NanoFoil-heated thermal battery stack were found to be in much lower quantities than those generated by the traditional thermal batteries and by batteries with other technologies. Other benefits of the NanoFoil-heated thin-film thermal battery technology included flexibility in form factor, as all the components in the stack—cathode, anode/electrolyte, NanoFoil, and buffer—can be cut into any desired shapes, and reduced height of the stack, as all the necessary components in a NanoFoil-heated thin-film thermal battery stack are significantly thinner than their counterparts in the traditional pressed pellet thermal battery stack.

5. References

1. Lamb, C. M. in: *Linden's Handbook of Batteries, 4th ed.*; Reddy, T. B.; Linden, D., eds.; McGraw-Hill Companies, Inc., New York, 2011, p. 36.1.
2. Guidotti, R. A.; Masset, P. *J. Power Sources* **2006**, *161*, 1443.
3. Ding, M. S.; Krieger, F. C.; Swank, J. A.; Poret, J. C.; McMullan, C. W.; Chen, G. *Use of NanoFoil as a New Form of Heat Source in Thermal Batteries*; ARL-TR-6141; U.S. Army Research Laboratory: Adelphi, MD, 2012.
4. Ding, M. S.; Krieger, F. C.; Swank, J. A.; Janow, C. W.; Delnick, F. M.; Branson, E. D. *Proc. 45th Power Sources Conference*, Las Vegas, NV, June 11–14, 2012, p. 623.
5. Jayaraman, S.; Knio, O. M.; Mann, A. B.; Weihs, T. P. *J. Appl. Phys.* **1999**, *86*, 800.
6. Gavens, A. J.; Van Heerden, D.; Mann, A. B.; Reiss, M. E.; Weihs, T. P. *J. Appl. Phys.* **2000**, *87*, 1255.
7. Ding, M. S.; Krieger, F. C.; Swank, J. A.; Poret, J. C.; Chen, G.; McMullan, C. W. *Proc.*, p. 635.
8. Ding, M. S.; Krieger, F. C.; Swank, J. A.; Poret, J. C.; McMullan, C. W.; Chen, G. *Proc. 43rd Power Sources Conference*, Philadelphia, PA, July 7–10, 2008, p. 615.
9. Ding, M. S.; Krieger, F. C.; Swank, J. A.; McMullan, C. W.; Chen, G.; Poret, *J. Proc. 43rd Power Sources Conference*, Philadelphia, PA, July 7–10, 2008, p. 377.
10. Krieger, F. C.; Poese, B. A.; Ding, M. S. *Proc. 45th Power Sources Conference*, Las Vegas, NV, June 11–14, 2012, p. 551.
11. Krieger, F. C.; Mullins, J. C.; Poese, B. A.; Ding, M. S.; Amabile, K. M.; Dratler, R.; Poret, J. C.; Janow, C. W. *Proc. 44th Power Sources Conference*, Las Vegas, NV, June 14–17, 2010, p. 517.

NO. OF COPIES	ORGANIZATION
1 (PDF)	DEFENSE TECHNICAL INFORMATION CTR DTIC OCA
2 (PDFS)	DIRECTOR US ARMY RESEARCH LAB RDRL CIO LL IMAL HRA MAIL & RECORDS MGMT
1 (PDF)	GOVT PRINTG OFC A MALHOTRA
6 (PDFS)	US ARMY ARDEC ATTN RDAR-EIF C JANOW ATTN RDAR-MEF-S C MCMULLAN ATTN RDAR-MEF-F B ARMSTRONG ATTN RDAR-MEF-F R DRATLER ATTN RDAR-MEF-F K AMABILE ATTN RDAR-MEF-F M ALLENDE
3 (PDFS)	US ARMY AMRDEC ATTN RDMR-WDP-C W MCMAHAN ATTN RDMR-WSA M TEMMEN ATTN RDMR-WSI M SANGHADASA
2 (PDFS)	SANDIA NATIONAL LABORATORIES ATTN E BRANSON ATTN C APBLETT
3 (PDFS)	US ARMY RSRCH LAB ATTN RDRL-SED-C F KRIEGER ATTN RDRL-SED-C J SWANK ATTN RDRL-SED-C M DING